Biochemical Pharmacology 80 (2010) 205–217

Contents lists available at ScienceDirect

Biochemical Pharmacology

journal homepage: www.elsevier.com/locate/biochempharm

Carbonylation of myosin heavy chains in rat heart during diabetes

Chun-Hong Shao [a], George J. Rozanski [b], Ryoji Nagai [c], Frank E. Stockdale [d], Kaushik P. Patel [b], Mu Wang [e], Jaipaul Singh [f], William G. Mayhan [b], Keshore R. Bidasee [a,g,*]

[a] Department of Pharmacology and Experimental Neuroscience, University of Nebraska Medical Center, Omaha, NE 68198-5800, United States
[b] Department of Cellular and Integrative Physiology, University of Nebraska Medical Center, Omaha, NE 68198-5850, United States
[c] Department of Food and Nutrition, Laboratory of Nutritional Science and Biochemistry, Japan Women's University, 2-8-1 Mejirodai, Bunkyo-ku, Tokyo, Japan
[d] Division of Oncology, Stanford University School of Medicine, Stanford, CA, United States
[e] Indiana University School of Medicine, Indianapolis, IN 46222, United States
[f] School of Forensic and Investigative Science, University of Central Lancashire, Preston, PR1 2He, UK
[g] Department of Environmental, Occupational and Agricultural Health, University of Nebraska Medical Center, Omaha, NE 68198-5800, United States

ARTICLE INFO

Article history:
Received 29 December 2009
Accepted 23 March 2010

Keywords:
Rat
Streptozotocin
Diabetes
Myosin heavy chain
Contractility
Carbonyl adducts
Reactive carbonyl species

ABSTRACT

Cardiac inotropy progressively declines during diabetes mellitus. To date, the molecular mechanisms underlying this defect remain incompletely characterized. This study tests the hypothesis that ventricular myosin heavy chains (MHC) undergo carbonylation by reactive carbonyl species (RCS) during diabetes and these modifications contribute to the inotropic decline. Male Sprague–Dawley rats were injected with streptozotocin (STZ). Fourteen days later the animals were divided into two groups: one group was treated with the RCS blocker aminoguanidine for 6 weeks, while the other group received no treatment. After 8 weeks of diabetes, cardiac ejection fraction, fractional shortening, left ventricular pressure development (+d*P*/d*t*) and myocyte shortening were decreased by 9%, 16%, 34% and 18%, respectively. Ca^{2+}- and Mg^{2+}-actomyosin ATPase activities and peak actomyosin syneresis were also reduced by 35%, 28%, and 72%. MHC-α to MHC-β ratio was 12:88. Mass spectrometry and Western blots revealed the presence of carbonyl adducts on MHC-α and MHC-β. Aminoguanidine treatment did not alter MHC composition, but it blunted formation of carbonyl adducts and decreases in actomyosin Ca^{2+}-sensitive ATPase activity, syneresis, myocyte shortening, cardiac ejection fraction, fractional shortening and +d*P*/d*t* induced by diabetes. From these new data it can be concluded that in addition to isozyme switching, modification of MHC by RCS also contributes to the inotropic decline seen during diabetes.

1. Introduction

Approximately 250 million people worldwide have diabetes mellitus (DM) and this number is expected to reach near 400 million by 2030 [1,2]. The situation is equally disturbing in the United States where about 9% of the population has DM [3]. Even more worrying is the three to five fold higher rates of cardiovascular diseases, including heart failure in these individuals in coming decades. Diabetic cardiomyopathy (DC) starts as an asymptomatic slowing in cardiac relaxation kinetics [4]. As the syndrome progresses, inotropy, fraction shortening and ejection fraction decline leading to an increase in morbidity and mortality [5]. To date, the etiology underlying these cardiac contractile defects remains incompletely characterized.

Myosin heavy chain (MHC) is the motor protein responsible for force generation. It is part of the myosin complex that is made up of six polypeptides: two MHC (≈220 kDa) isozymes intertwined at their tails with theirs heads separated and containing one essential light chain (≈18 kDa) and one regulatory light chain (≈22 kDa) [6]. The myosin complex is divided into three functionally distinct regions: a motor and a lever arm domain that are located in the globular head and a tail or rod domain. The motor domain contains the ATP binding pocket and the actin-binding site [7,8]. The lever arm consists of two IQ motifs that form attachment sites for the essential and regulatory light chains. The tail region forms the thick filaments of muscle sarcomere. Following depolarization, Ca^{2+} released from the internal sarcoplasmic reticulum (SR) bind to troponin C that resides on actin filaments. Ca^{2+} binding to troponin C alters its conformation and increases its affinity for troponin I [9]. The increased troponin C-troponin I interaction creates an opening that allows MHC to bind and form weak cross-bridges with actin. The binding of MHC to actin exposes its nucleotide-binding pocket, allowing ATP to bind. Following ATP binding, a narrow cleft between the upper and lower domains of the motor head on MHC

* Corresponding author at: 985800 Nebraska Medical Center, Durham Research Center, DRC 3047, Omaha, NE 68198-5800, United States. Tel.: +1 402 559 9018; fax: +1 402 559 7495.
E-mail address: kbidasee@unmc.edu (K.R. Bidasee).

0006-2952/$ – see front matter © 2010 Elsevier Inc. All rights reserved.
doi:10.1016/j.bcp.2010.03.024

opens, reducing MHC affinity for actin. Immediately after detaching, hydrolysis of ATP occurs resulting in the formation of a metastable ternary complex between myosin, ADP and inorganic phosphate (P_i). The release of P_i reinitiates strong binding of the motor head of MHC to actin. Elastic bending and interaction of the essential light chains with actin induces the power stroke (force generation). During the power stroke, conformational changes induced by ATP are reversed, the nucleotide-binding pocket reopens, ADP is released and the rigor conformation is reestablished to restart the process [8,10]. Thus, a series of well-timed MHC conformational changes are needed to ensure effective contraction.

Two isoforms of MHC are expressed in mammalian heart: MHC-α and MHC-β. In healthy adult rodents, MHC-α is the dominant isozyme. Following stressors like diabetes, MHC isozymes switch such that MHC-β becomes the dominant heart isozyme [11,12]. This switching starts as early as 1 week after the induction of DM as a result of reductions in production and circulation of thyroid hormones [13,14]. Since the ATPase activity of MHC-β is two-to-three fold less than that of MHC-α, studies attribute the reduction in inotropy seen during diabetes, in part to MHC isozyme switching [11–14]. However, in animals models of diabetes including the widely used streptozotocin-induced type 1 diabetic rat model, measurable decline in cardiac inotropy typically starts after 2–3 weeks of diabetes and progresses as the duration of diabetes increases [15,16]. Moreover, intensive lowering of blood glucose does not prevent the inotropic decline in patients with diabetes mellitus [17,18]. This and other data prompted us to investigate whether factors other than isozyme switching may be further reducing MHC activities and cross-bridge kinetics during diabetes.

Shortly after the onset of hyperglycemia, production of reactive carbonyl species (RCS) increases as a result of enhanced glucose and fatty acid oxidation and increased expression of RCS generating enzyme serum semicarbazide amine oxidases [19,20]. These electrophiles can react with the exposed amine/azide group of basic residues on proteins to form carbonyl adducts [21] by a process referred to as carbonylation. For proteins like MHC that have slow a turn over rate of >5 days [22], adducts will accumulate over time. More than 20 years ago, Yudkin et al. [23] found elevated levels of glucose adducts (glycosylation) on MHC from post-mortem hearts of diabetic patients. Others have since confirmed these findings [24–26]. What remains incompletely defined to date is whether other types of carbonyl adducts are formed on MHC during DM and whether the presence of these adducts compromise the rate at which MHC hydrolyzes ATP to generate the power stroke. Thus, the objectives of present study were three fold: (i) to assess whether other carbonyl adducts are formed on MHC during DM, (ii) to determine which amino acid residues on MHC susceptible to carbonylation, and (iii) to determine if carbonyl adducts formed on MHC during diabetes impair ATP hydrolyze and cross-bridge formation with actin.

2. Materials and methods

2.1. Chemicals and drugs

Ketamine (Ketaset®) was obtained from Fort Dodge Animal Health, Fort Dodge, IA, USA, acepromazine from Boehringer Ingelheim Vetmedica Inc., (St. Joseph, MO). Aminoguanidine bicarbonate, Na_2-ATP and Inactin® were obtained from Sigma–Aldrich (St. Louis, MO). mAb F59 and mAb S58 monoclonal antibodies used to detect total MHC (MHC-α and MHC-β and MHC were obtained from The Developmental Studies Hydridoma Bank, University of Iowa, Iowa City, IA. Actin (C-11), anti-goat, and anti-mouse IgG-horseradish peroxidase were purchased from Santa Cruz Biotechnology (Santa Cruz, CA). Collagenase type 2 was obtained from Worthington Biochemical Corp., Lakewood, NJ. Serum T3 was measured in triplicate by radioimmunoassay kits (Diagnostic Products Corporation, Los Angeles, CA), total thiobarbituric acid reactive substances (TBARS) were assayed using OXI-TEK (TBARS) assay kits (Zepto Metric Corporation, Buffalo, NY) and serum semicarbazide-sensitive amine oxidase was assayed using SSAO assay kits (Cell Technology, Inc., Mountain View, CA). Insulin pellets were obtained from LinShin Canada Inc., Scarborough, CANADA. Standard reagents and buffers used were of the highest grade available and also purchased from Sigma–Aldrich (St. Louis, MO).

2.2. Induction and verification of experimental type 1 diabetes mellitus

Animals used for the study were approved by the Institutional Animal Care and Use Committee, University of Nebraska Medical Center and adhered to APS's Guiding Principles in the Care and Used of Animals [27]. Eighty-four male Sprague–Dawley rats (≈200 g) were purchased from Sasco Breeding laboratories (Omaha, NE). Laboratory chow and tap water were given *ad libitum*. After acclimatization for 1 week, 50 rats were given a single intraperitoneal (i.p.) injection (0.25 mL) with freshly prepared streptozotocin (STZ) in a 2% solution of cold 0.1 M citrate buffer, pH 4.5 (45–50 mg/kg) as described earlier [28]. The other 34 rats were injected with a similar volume of citrate buffer only. Throughout the experimental protocol, blood glucose levels of diabetic animals were maintained between 19.2–25 mmol (350–450 mg/dL) by inserting 0.5 mm × 2 mm insulin pellets subcutaneously. To generate euglycemic diabetic controls, 0.5 mm × 5 mm insulin pellets were inserted after 6 weeks of diabetes. The latter is referred to as the insulin therapy group. Animals were housed in pairs of similar weights to minimize dominance at 22 °C with fixed 12 h light/12 h dark cycles and 30–40% relative humidity.

2.3. Treatment to reduce reactive carbonyl species (RCS)

Two weeks after STZ injection, diabetic rats were randomly divided into three groups. One group of was placed on aminoguanidine (Ag) treatment (1.0 g/L/day, 0.1%) via drinking water for 6 weeks [29]. A second group was treated with insulin after 6 weeks of diabetes to attain euglycemia and the third group remained untreated. Control animals were also divided into two groups: one group was placed on Ag treatment at a higher dose of 1.5 g/L for 6 weeks while the other remained as untreated. The higher dose of Ag was used for treating control rats as we earlier found that they drink about 66% less water per day than diabetic rats (150 mL/day *vs* 400 mL/day). Ag was selected for this study because of the multiple mode by which it inhibits RCS.

2.4. Assessment of cardiac function in vivo

2.4.1. M-mode echocardiography

M-mode echocardiography was performed at the end of the 8-week protocol in lightly anesthetized (0.3 mL of a cocktail containing 100 mg/ml ketamine and 10 mg/mL acepromazine given i.p.) animals using an Acuson Sequoia 512C ultrasound system (Siemens) with a 15L8 probe as described earlier [28]. Left ventricular end-diastolic diameter (LVEDD), end-systolic diameter (LVESD), left ventricular end-diastolic volume (LVEDV) and end-systolic volume (LVESV) were measured parameters. Percent fractional shortening (FS) was calculated as FS = [(LVEDD − LVESD)/LVEDD] × 100. Percent ejection fraction (EF) was also calculated as EF = [(LVEDV − LVESV)/LVEDV] × 100.

2.4.2. In vivo hemodynamics

Basal and isoproterenol-stimulated heart rates, left ventricular pressures, left ventricular end-diastolic pressures and rates of change of left ventricular pressures ($\pm dP/dt$) were also evaluated in anesthetized rats at the end of the 8-week protocol as described previously [28]. In this study, two bolus doses of isoproterenol (0.1 and 0.25 μg/kg) were administered 35 min apart. A powerlab data acquisition system (ADInstuments, Colorado Springs, CO) was used for acquiring the data. Hemodynamic parameters were then extracted and Mircosoft Excel (Microsoft Corp., Seattle, WA) and Prism GraphPad (San Diego, CA) were used for analysis of the data.

2.5. Heart and blood collection

At the end of the *in vivo* studies, animals were euthanized (Inactin® 75 mg/kg i.p.), abdominal cavities were opened and blood samples were collected via left renal arteries for analysis of terminal plasma glucose, insulin, T3 levels, thiobarbituric acid reactive substances (TBARS, used as a measure of serum levels of RCS), % glycosylated hemoglobin and serum semicarbazide-sensitive amine oxidase (SSAO) activity (used as an index of the amount of the RCS, methylglyoxal). Thereafter, the chest cavity of each rat was opened and heart was rapidly removed and placed in isolation buffer for extraction of actomyosin.

2.6. Isolation of myocytes

For myocyte isolation, animals were injected ten min prior to Inactin® injection with heparin (1000 U/kg, i.p.). After euthanasia, chest cavities were opened, and hearts were rapidly removed and placed in Krebs–Henseleit buffer. Thereafter, hearts were cannulated and perfused retrograde in a Langendorff's apparatus with collagenase. Cells were used within 5–6 h following isolation [28,30].

2.7. Myocyte contractile kinetics

Myocyte contractile kinetics was assessed using a high-speed video-based edge detection system (IonOptix Corporation, Milton, MA) as described previously [28,30], except that cells were field stimulated (10 V) for 10 ms at 0.5, 1.0 and 2.0 Hz. Contractions were recorded using data acquisition software (IonOptix Corporation, Milton, MA). Rates of myocyte shortening and re-lengthening and extent of cell shortening were then calculated using IonWizard version 5.0.

2.7.1. Relative levels of MHC mRNA

Semi-quantitative reverse transcription polymerase chain reactions (RT-PCR) were used to determine steady-state levels of RNA encoding MHC as described by Danzi et al. [31]. For this, total RNA (tRNA) was isolated from ventricular tissues. After isolation, equivalent amounts of tRNA were reverse transcribed using primers that anneal to the first intron of the MHC-α gene (MHC-α: reverse 5′-$_{949}$GACACAGAAAGAAAGGAAGGAT-3′) or to the first intron of the MHC-β gene (reverse: 5′-$_{1456}$ACACACGCGCACACACTAGCA-3′). Thereafter, PCR reactions were carried out to determine relative levels of MHC-α and MHC-β using isozyme specific primers; MHC-α, sense 5′-$_{614}$ATTTCTCCATCCCAAGTAAG-3′ and antisense, 5′-$_{949}$GACACAGAAAGAAAGGAAGGAT-3′; MHC-β, sense, 5′-$_{1144}$TGAGCATTCT-CCTGCTGTTTC-3′ and antisense, 5′-$_{1456}$ACA-$_{1456}$ACACACGCGCACACACTAGCA-3′. β actin was also amplified and used as an internal reference using primers; sense 5′-$_{254}$CACTGTC-$_{254}$CACTGTCGAGTCCGCGTCCAC-3′ and antisense 5′-$_{492}$GGAATAC-$_{492}$GGAATACGACTGCAAACACTC-3′. Reaction protocols: 5 min denaturing (94 °C): 1 min annealing (46 °C for MHC-α, 56.7 °C for MHC-β and β-actin): 2 min extension (72 °C), were repeated for a total of 35 cycles.

2.7.2. Isolation of actomyosin

Actomyosin gels were isolated using a modification of the procedure described by Ash et al. [32]. Briefly, ventricular tissues (right and left) from each heart was cut into small pieces and homogenized in 15 mL of 10 mM $NaHCO_3$ with 5 mM Na-azide using a Polytron (setting 5, Pro Scientific Inc., Oxford, CT). Homogenates were then centrifuged at 7000 × *g* for 20 min and pellets were resuspended in 10 mL of 600 mM KCl and placed in a refrigerated room (4 °C) for 16 h. The next day, viscous suspensions were centrifuged at 30,000 × *g* for 20 min and supernatants were gently decanted and diluted with two volumes of 0.3 mM $NaHCO_3$ to give a final KCl concentration of 0.2 M. Samples were then centrifuged at 6000 × *g* for 20 min, and soft pellets were resuspended in two volumes of 0.8 M KCl and re-centrifuged at 37,000 × *g* for 30 min. Three volumes of 0.3 mM $NaHCO_3$ were then slowly added to supernatants over a period of 20 min maintaining continuous mixing with a magnetic stirrer. Actomyosin pellets were collected by centrifugation at 6000 × *g* for 20 min and resuspended by stirring in 2 mL of 1.0 M dithiothreitol to reduce disulfide bonds and prevent oxidation. Protein concentrations were determined and samples used within 4 h of isolation for functional studies.

2.7.3. Relative levels of MHC protein

Western blots were used to determine relative levels of MHC-α, MHC-β in hearts from control, STZ-induced diabetic, Ag-treated and insulin-treated animals as described earlier [28,30] using 0.5 μg (or 5.0 μg for actin) of actomyosin gel electrophoresed on 4–15% linear gradient polyacrylamide gels for 2.5 h at 150 V. Polyvinylidene difluoride membranes containing transferred proteins were incubated for 20 h at 4 °C with 1:1500 primary antibodies (mAb F59 for total MHC; mAb S58 for MHC-β or C-11 for actin) followed by 2 h at room temperature with secondary antibodies (anti-mouse IgG-horseradish peroxidase or anti-goat IgG-horseradish peroxidase). After this time, membranes were washed and incubated for 1 min with enhanced chemiluminescence (ECL) and exposed to X-ray films. Autoradiograms were developed after 10–20 s. Relative intensities of the signals were measured using Scion Image 1.62c.

2.8. Syneresis

Actomyosin gels prepared as described above contain about 5–10 μM free Ca^{2+} and when ATP is added they undergo shrinkage or syneresis [32] which could be determined spectroscopically. For this, actomyosin gels (0.5 mg/mL) were resuspended in buffer containing 50 mM KCl, 1 mM $MgCl_2$, 20 mM Tris–maleate (pH 7.0). Samples were then placed in cuvettes and basal absorbances were measured at 660 nm using a UV/vis spectrophotometer (Burlingame, CA). After this, 1 mM Na_2-ATP was added and absorbance changes were monitored. In separate experiments, 0.03 mM EGTA was added prior to addition of Na_2-ATP and changes in absorbance were measured. Ca^{2+}-sensitive-syneresis was determined from change in absorbance with and without EGTA.

2.8.1. Actomyosin ATPase activity

Ca^{2+}- and Mg^{2+}-sensitive actomyosin ATPase activities were assessed using the procedure by Bhan and Scheuer [33], except that inorganic phosphate (P_i) generated from the hydrolysis of ATP, was assessed using the more sensitive malachite green colorimetric assay [34]. Data are expressed as micromoles of inorganic phosphate (P_i) liberated per 100 μg protein per 10 min.

2.9. Mass spectrometry

2.9.1. Sample preparation

Coomassie-stained myosin bands were excised from polyacrylamide gels, cut into small pieces, destained with 50% acetonitrile/

50 mM ammonium bicarbonate, reduced with 10 mM dithiothreitol, and then alkylated with 55 mM iodoacetamide as described earlier [35,36]. After alkylation, gel pieces were digested overnight with trypsin (6 ng/nL; Promega Corporation, Madison, WI) at 37 °C. The next day, the peptides were desalted by eluting from micro C_{18}-ZipTip columns (Millipore, Bedford, MA) with a solution of 50% acetonitrile and 0.1% trifluoroacetic acid and separated into two aliquots.

2.9.2. MALDI-TOF acquisition

α-Cyano-4-hydroxycinnamic acid was added to one aliquot and matrix-assisted laser desorption/ionization-time of flight (MALDI-TOF) mass spectra were recorded in the positive reflectron mode (Micromass, Manchester, UK) [35,36]. Internal calibration was performed using auto digestion peaks of bovine trypsin (monoisotopic mass [M+H$^+$], m/z 842.5099 and m/z 2211.1045) before analysis of experimental samples. Peptides were assigned using ProteinLynx (Micromass), Profound (for PMF) and MASCOT (web-based database search engine).

2.10. Mining MALDI-TOF data

MALDI-TOF mass data files were uploaded onto Profound (http://prowl.rockefeller.edu/) and M+H$^+$ were assigned to MHC peptides. An in-house PERLscript was then used to search the MALDI-TOF mass data files to determine if any of the M+H$^+$ represent MHC peptides modified with carbonyl adducts, and if so, what type of adduct and where they are located on protein. For this, rat MHC-α (GenBank accession no. NP_058935) and MHC-β (GenBank accession no. NP_058936) were digested *in silico* using Expasy (http://ca.expasy.org/tools/peptide-mass.html) and M+H$^+$ of all possible peptides (including cysteine with iodoacetamide and acrylamide adducts, oxidized methionines, and two miscleavage products) were uploaded into the PERL algorithm along with the MALDI-TOF mass data files. Data files were then searched to determine if any of the experimentally obtained M+H$^+$ were greater than theoretical M+H$^+$ of miscleaved MHC peptides by a specific delta mass (ΔM). As an example, an increase of 58.02 Da could reflect a miscleaved peptide modified with N^{ε}-(carboxymethyl)-lysine adduct (CML); an increase of 58.03 Da, a pentosidine adduct; an increase of 144.03 Da, an imidazolone A adduct; an increase of 142.03 Da, an imidazolone B adduct; an increase of 108.02 Da, a pyrraline adduct; an increase of 270.07 Da, a 1-alkyl-2-formyl-3,4-glycosyl pyrrole (AFGP) adduct and an increase of 162.02, an Amadori adduct (rearranged glucose). We also ensured that the correct basic residue was present in the miscleaved peptide. For example, if a miscleaved peptide was assigned with an imidazolone adduct, it must have a miscleaved arginine as this residue form imidazolone adducts. If it was assigned with a CML, pyralline or AGFP, it must have a miscleaved lysine. For cross-linking pentosidine adducts, one of the peptide must have a miscleaved lysine and other must have a miscleaved lysine.

2.10.1. Confirmation of peptide sequences

The second aliquot from trypsin digestion was subjected to liquid chromatography–mass spectrometry (LC–MS) analyses using a nanoflow capillary liquid chromatography system coupled with a quadruple time of flight (Q-TOF) mass spectrometer (Micromass, Manchester, UK) fitted with a Z-spray ion source. Samples were concentrated using an online pre-column (C_{18}, 0.3 mm i.d., 5 cm length) while separation of the peptides was carried out on a reverse-phase capillary column (Pepmap C_{18}, 75 mm i.d., 15 cm length; LC Packings, San Francisco, CA) running at 300 nL/min. The mobile phase gradient consisted of a linear gradient from 100% A (0.1% formic acid/3% acetonitrile/96.9% H_2O, v/v) to 70% B (0.1% formic acid/2.9% H_2O/97% acetonitrile, v/v) in 50 min followed by a linear gradient to 100% B in 10 min. Mass spectra were acquired in positive ion mode. Collision-induced dissociation (CID) product ion MS/MS spectra obtained was processed using MassLynx (Micromass, UK) software to confirm amino acid sequences. MASCOT search engine (http://www.matrixscience.com/search_form_select.html) was also used.

2.11. Pentosidine adducts on MHC

Western blots employing pentosidine antibodies [37] were used to further confirm the presence of this specific adduct on MHC. For this, 1.5 μg actomyosin proteins from the five samples were solubilized with gel-dissociation medium and electrophoresed on 4–20% linear gradient polyacrylamide gels for 2.5 h at 150 V. The proteins were then transferred at 4 °C overnight onto polyvinylidene difluoride membranes at 100 mA and Western blot analyses were carried out employing standard procedures described above using mouse monoclonal anti-pentosidine antibodies. After transfer, polyacrylamide gels were also stained with Coomassie Blue dye and destained with 25% methanol/1% acetic acid to ensure equal protein load.

2.12. Statistical analyses

Data shown are means ± standard errors of the mean (SEM). Differences among values from each of the five groups (control (C), STZ-induced diabetic (D), Ag-treated control (Ag-C), Ag-treated STZ-diabetic (Ag-D) and insulin-treated STZ-diabetic (Ins-D)) were evaluated using two-way ANOVA employing Prism 5 (GraphPad Software, Inc. San Diego, CA). The results were considered significantly different if $p < 0.05$.

3. Results

3.1. Animal characteristics

The general characteristics of the animals used in this study are shown in Fig. 1. Panel A shows longitudinal changes in body mass and blood glucose levels of C, D, Ag-C, Ag-D and Ins-D rats. Standard errors were less than ≤5% and left out of data points for clarity. Table shows serum marker assayed in this study. Two weeks of insulin therapy (euglycemia) starting 6 weeks after the onset of diabetes, increased body mass and plasma insulin level, and lowered blood glucose, % hemoglobin glycosylation, serum SSAO, and thiobarbituric acid reactants to near control, non-diabetic levels, establishing that seen were the result of diabetes and not from STZ toxicity.

3.2. In vivo left ventricular function

3.2.1. M-mode echocardiography

Fig. 2 shows representative M-mode echocardiograms and the average hemodynamic parameters of C, D, Ag-C, Ag-D and Ins-D rats. Compared with non-diabetic controls, diabetic rats were bradycardic. STZ-diabetic animals also exhibited significant ($p < 0.05$) reductions in ejection fraction, fractional shortening and cardiac output. Mean left ventricular end-diastolic (LVEDD) and systolic (LVESD) diameters were also significantly ($p < 0.05$) larger in STZ-diabetic animals than in age-matched control animals. Diabetes did not alter mean aortic diameter (data not shown). Unlike insulin therapy, treatment of diabetic rats with Ag for up to 6 weeks did not attenuate the bradycardia induced by diabetes, however it blunted reductions in fractional shortening, ejection fraction and LVESD. There was no significant difference in LVEDD between D and Ag-D animals. Treating control rats with Ag for 6 weeks had no significant effect on measured and derived

(A)

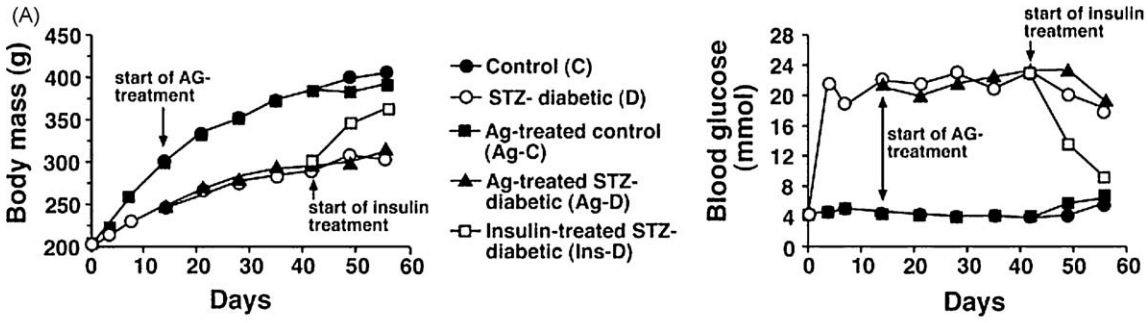

(B)

Parameter	Control (C) (n = 9)	STZ-diabetic (D) (n = 9)	Aminoguanidine-treated control (Ag-C) (n = 9)	Aminoguanidine-treated STZ-diabetic (Ag-D) (n = 9)	Insulin-treated STZ-diabetic (Ins-D) (n= 8)
Glycosylated hemoglobin (%)	3.89 ± 0.08	9.34 ± 0.83*	4.23 ± 0.21	9.48 ± 0.67	5.72 ± 0.93**
Serum Insulin (ng/mL)	0.68 ± 0.07*	0.33 ± 0.04*	0.67 ± 0.07	0.31 ± 0.03	0.57 ± 0.01
Serum T3 (ng/dL)	227.2 ± 14.9	150.3 ± 20.1*	204.1 ± 14.5	162.0 ± 26.2	ND
Serum TBARS (nmol/mL)	2.4 ± 0.3	11.1 ± 1.9*	4.1 ± 0.9#	7.2 ± 0.7**	4.14 ± 0.95**
Serum SSAO activity (units/mL/min)	0.32 ± 0.02	0.53 ± 0.03*	0.47 ± 0.03#	0.41 ± 0.05**	0.34 ± 0.06**

Fig. 1. General characteristics of animals used in this study. Panel A shows longitudinal changes in body mass and blood glucose. SEM were ≤5% and left out for clarity. Table below in (B) shows the serum profile of select markers. TBARS, total thiobarbituric acid reactive substances; SSAO, serum semicarbazide amine oxidase. Values shown are mean ± SEM ($n \geq 8$). (*) Significantly different from control ($p < 0.05$). (**) Significantly different from STZ-diabetic ($p < 0.05$).

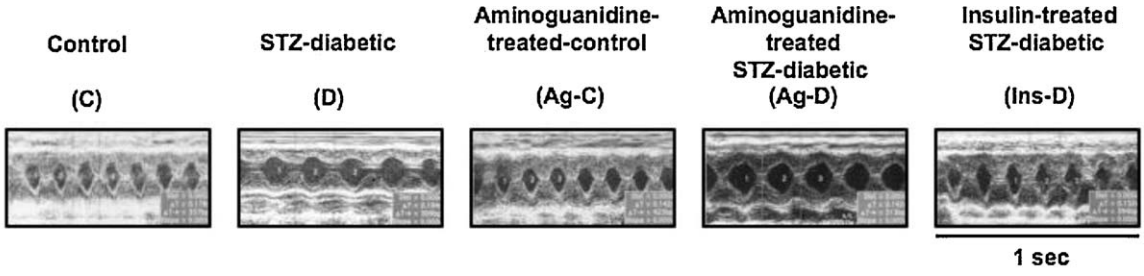

Parameter	Control (C) (n = 9)	STZ-diabetic (D) (n = 9)	Aminoguanidine-treated control (Ag-C) (n = 9)	Aminoguanidine-treated STZ-diabetic (Ag-D) (n = 9)	Insulin-treated STZ-diabetic (Ins-D) (n = 9)
Heart rate (beats per min)	384.5 ± 27.6	291.8 ± 23.6*	417.0 ± 19.8	294.1 ± 30.2	357.6 ± 23.3
LVEDD[1]	6.19 ± 0.30	6.89 ± 0.27*	6.31 ± 0.29	6.68 ± 0.15	6.44 ± 0.27
LVESD[2]	2.67 ± 0.28	3.41 ± 0.35*	2.78 ± 0.17	2.74 ± 0.13**	2.80 ± 0.14**
% Fractional shortening	60.7 ± 2.9	51.1 ± 1.7*	57.96 ± 3.4	57.9 ± 1.9**	56.4 ± 3.7**
% Ejection fraction	84.1 ± 2.3	76.5 ± 3.9*	81.8 ± 2.9	83.3 ± 1.5**	82.3 ± 1.2**
Stroke volume (mL)	0.31 ± 0.22	0.35 ± 0.01*	0.32 ± 0.01	0.32 ± 0.02	0.30 ± 0.03
Cardiac output (mL/min)	117.0 ± 11.7	94.5 ± 0.7*	132.5 ± 6.4	94.1 ± 5.1	107.3 ± 10.3**

Fig. 2. Upper panels show representative M-mode echocardiograms from control (C), STZ-diabetic (D), Ag-treated control (Ag-C), Ag-treated STZ-diabetic (Ag-D) and insulin-treated STZ-diabetic (Ins-D) rats. Three loops of M-mode were captured for each animal. Values in table below are mean ± SEM (n = p). [1]LVEDD – left ventricular end-diastolic diameter. [2]LVESD – left ventricular end-systolic diameter. (*) Significantly different from controls ($p < 0.05$). (**) Significantly different from STZ-diabetic ($p < 0.05$).

Table 1
In vivo hemodynamic parameters of hearts from control (C), STZ-diabetic (D), Ag-treated control (Ag-C), Ag-treated STZ-diabetic (Ag-D) and insulin-treated STZ-diabetic (Ins-D) rats. Values shown are mean ± SEM ($n = 8$, from each group).

Parameter	Control (C) ($n = 8$)	STZ-diabetic (D) ($n = 8$)	Aminoguanidine-treated control (Ag-C) ($n = 8$)	Aminoguanidine-treated STZ-diabetic (Ag-D) ($n = 8$)	Insulin-treated STZ-diabetic (Ins-D) ($n = 8$)
Heart rate (bpm)					
Before ISO	338.6 ± 8.5	268.1 ± 118.6*	314.6 ± 10.8'	273.1 ± 32.8	273.1 ± 32.8
0.1 pg/kg ISO	385.5 ± 12.2	377.6 ± 34.2	362.7 ± 15.3	326.5 ± 31.9	404.1 ± 4.3
0.25 pg/kg ISO	395.8 ± 12.6	343.1 ± 14.9*	363.1 ± 16.8	333.0 ± 33.9	402.9 ± 4.9
Systolic BP (mm Hg)[a]					
Before ISO	136.1 ± 10.2	111.2 ± 13.6*	149.8 ± 8.7	109.1 ± 18.7	138.6 ± 4.0**
0.1 pg/kg ISO	151.8 ± 8.1	129.8 ± 13.5*	162.7 ± 10.8	127.1 ± 19.6	157.1 ± 1.2**
0.25 pg/kg ISO	149.3 ± 6.9	132.3 ± 10.8	154.9 ± 10.4	124.9 ± 18.2	155.1 ± 5.3**
Peak LVP (mm Hg)[b]					
Before ISO	133.6 ± 9.4	104.7 ± 6.2*	135.2 ± 8.6	118.4 ± 7.6**	133.9 ± 2.8**
0.1 pg/kg ISO	133.2 ± 4.4	98.7 ± 7.5*	128.7 ± 7.1	114.9 ± 7.7**	138.0 ± 1.6**
0.25 pg/kg ISO	129.9 ± 4.3	95.3 ± 7.1*	131.3 ± 6.5	108.1 ± 7.4	123.9 ± 4.6**
LVEDP (mm Hg)[c]					
Before ISO	0.1 ± 0.4	6.6 ± 1.6*	2.1 ± 0.3*	0.5 ± 1.3**	2.0 ± 2.1**
0.1 pg/kg ISO	1.9 ± 0.8	4.4 ± 1.1	1.4 ± 0.7	2.5 ± 0.5**	2.1 ± 1.8
0.25 pg/kg ISO	2.3 ± 0.9	2.1 ± 0.4*	0.9 ± 0.7	2.7 ± 0.6	1.8 ± 0.2
+d*P*/d*t* (mm Hg/s)[d]					
Before ISO	9954.5 ± 900.5	6521.4 ± 91 3.6-	11125.9 ± 772.3	9000.7 ± 921.7**	11209.2 ± 450.7**
0.1 pg/kg ISO	14971.1 ± 1653.4	12659.4 ± 1391.6	17435.4 ± 1771.1	14633.1 ± 708.1	16057.0 ± 525.3**
0.25 pg/kg ISO	15575.3 ± 1655.7	13067.7 ± 1077.9	17227.1 ± 1697.7	13202.5 ± 1173.8	16329.4 ± 834.3**
−d*P*/d*t* (mm Hg/s)[e]					
Before ISO	8065.5 ± 995.5	5279.6 ± 1096.5'	8983.3 ± 922.1	6777.5 ± 1136.7	7583.9 ± 528.9**
0.1 pg/kg ISO	9859.6 ± 988.2	7717.3 ± 1275.3*	11386.3 ± 1302.9	8285.4 ± 1564.8	11445.4 ± 1525.5**
0.25 pg/kg ISO	10711.5 ± 1239.1	7904.8 ± 821.1'	10344.6 ± 1229.9	7431.1 ± 1981.1	10188.3 ± 1530.5**

[a] BP – blood pressure.
[b] LVP – left ventricular pressure.
[c] LVEDP–left ventricular end-diastolic pressure.
[d] +d*P*/d*t* – rate of change of left ventricular pressure increase.
[e] −d*P*/d*t* – rate of change of left ventricular pressure decrease.
* Significantly different control ($p < 0.05$).
** Significantly different from STZ-diabetic ($p < 0.05$).

echocardiographic parameters, although there were trends toward increases in heart rate and cardiac output.

3.2.2. *In vivo* hemodynamics

Table 1 shows mean hemodynamic parameters of control and STZ-induced diabetic rats with and without Ag treatment, as well as euglycemic diabetic controls before and after administration of isoproterenol, a β-adrenoceptor agonist. Consistent with echocardiography data, basal heart rates of Inactin®-anesthetized STZ-diabetic animals were significantly lower ($p < 0.05$) than those of control animals. Basal mean systolic blood pressure was also significantly lower (18.2 ± 3.2%), as was mean peak left ventricular pressure (LVP) and rates of left ventricular pressure changes (±d*P*/d*t*, Table 1). Left ventricular end-diastolic pressure (LVEDP) was elevated in STZ-diabetic animals (6.6 ± 1.6 mm Hg *vs* 2.1 ± 0.3 mm Hg, $p < 0.05$). When injected with 0.1 μg/kg isoproterenol, mean peak heart rate and +d*P*/d*t* of STZ-diabetic animals were similar to those of control animals. However, mean systolic blood pressure, peak LVP and −d*P*/d*t* remained lower than that of control animals. LVEDP also remained higher. Injecting a second higher dose of isoproterenol (0.25 μg/kg) resulted in similar hemodynamic trends, although in some cases there was evidence of β-adrenoceptor desensitization.

Treating diabetic animals with Ag did not change mean basal heart rate, systolic blood pressure and −d*P*/d*t*, but it blunted decreases in basal peak LVP and basal +d*P*/d*t* induced by diabetes. Ag-treated STZ-diabetic animals also had reduced LVEDP. Treating STZ-diabetic rats with Ag also increased basal and isoproterenol-stimulated peak LVP. On the other hand, treating control animals with Ag significantly lowered their mean basal heart rate ($p < 0.05$) and increased LVEDP. All other hemodynamic parameters remained essentially the same although there were trends toward increases in basal and isoproterenol-stimulated ±d*P*/d*t* (Table 1). Hemodynamic parameters of euglycemic diabetic animals were similar to that of control, non-diabetic animals.

3.3. Myocyte contractile kinetics

In earlier studies [28,30], we found that myocytes isolated from STZ-diabetic rats were less tolerant to Ca^{2+} reconstitution compared with myocytes from age-matched control rats. Treating STZ-diabetic animals with Ag minimized this Ca^{2+} intolerance and as a result, myocyte yields from Ag-treated animals were about 30% higher than those from STZ-diabetic animals. There were no significant differences in mean length of myocytes isolated from C, D, Ag-C, Ag-D and Ins-D rat hearts (Table 2). In this study cell capacitance was not measured. When stimulated at a frequency of 0.5 Hz, velocities of cell shortening and re-lengthening were significantly ($p < 0.05$) lower in myocytes from STZ-diabetic animals compared with myocytes from control animals. Extent of shortening was also 17% less in myocytes isolated from STZ-diabetic animals and times to 50% peak myocyte shortening and re-lengthening were significantly ($p < 0.05$) longer in the diabetic rats. Similar trends were also seen at higher stimulation frequencies (1.0 and 2.0 Hz), see Table 2.

Six weeks of Ag treatment, initiated 2 weeks after the onset of diabetes, blunted decreases in contractile velocities and extent in cell shortening seen with 0.5 and 2.0 Hz stimulation, although there were no changes at 1.0 Hz. The reason for the latter is not clear. Interestingly, while Ag treatment blunted the decrease in relaxation velocity at 0.5 Hz, it did not increase relaxation kinetics

Table 2
Contractile kinetics of ventricular myocytes isolated from control (C), STZ-diabetic (D), Ag-treated control (Ag-C), Ag-treated STZ-diabetic (Ag-D) and insulin-treated STZ-diabetic (Ins-D) rats. Values shown are mean ± SEM for ≥72 cells obtained from 5 separate animals from each group.

Parameter	Control (C) (n = 76)	STZ-diabetic (D) (n = 76)	Aminoguanidine-treated control (Ag-C) (n = 75)	Aminoguanidine-treated STZ-diabetic (Ag-D) (n = 80)	Insulin-treated STZ-diabetic (Ins-D) (n = 72)
Cell length (μm)	118.3 ± 2.1	116.8 ± 2.1	119.3 ± 3.5	115.8 ± 2.8	116.9 ± 2.3
Contraction velocity (μm/s)					
0.5 Hz	136.5 ± 6.0	83.0 ± 4.6*	124.8 ± 5.2	92.4 ± 3.8**	132.5 ± 5.8**
1.0 Hz	141.8 ± 7.8	89.6 ± 5.8*	122.5 ± 7.4	96.3 ± 5.3	126.3 ± 7.8**
2.0 Hz	128.1 ± 6.9	91.9 ± 5.3*	123.8 ± 8.7	106.6 ± 5.6**	132.3 ± 7.8**
Percent cell shortening					
0.5 Hz	12.0 ± .45	9.9 ± 0.5'	12.3 ± 0.4	10.5 ± 0.4**	12.4 ± 0.8**
1.0 Hz	12.5 ± 0.6	9.9 ± 0.6*	11.0 ± 0.5	10.1 ± 0.6	11.1 ± 0.6**
2.0 Hz	10 0 ± 0 4	8.8 ± 0.5*	10.3 ± 0.5	9.5 ± 0.5*	11.2 ± 0.6**
Relaxation velocity (μm/s)					
0.5 Hz	92.3 ± 5.4	71.6 ± 4.6*	95.8 ± 5.3	90.0 ± 3.1**	96.0 ± 5.6**
1.0 Hz	97.5 ± 6.8	76.8 ± 5.r	95.8 ± 7.4	84.0 ± 4.4	91.6 ± 6.4**
2.0 Hz	84.1 ± 5.1	82.1 ± 5.9	97.9 ± 8.6	89.7 ± 6.0	100.7 ± 9.7**
Time to 50% peak contraction (ms)					
0.5 Hz	63.1 ± 3.5	90.5 ± 4.0*	70.3 ± 2.1	73.7 ± 1.8**	63.6 ± 2.7**
1.0 Hz	65.9 ± 2.2	84.1 ± 2.1*	72.3 ± 2.4	71.7 ± 1.9**	69.1 ± 1.8**
2.0 Hz	52.5 ± 0.1	64.7 ± 1.6*	56.1 ± 0.8	58.3 ± 0.9**	52.6 ± 0.6**
Time to 50% peak relaxation (ms)					
0.5 Hz	402.2 ± 11.9	464.9 ± 12.1*	381.8 ± 9.6	417.5 ± 5.6**	359.5 ± 7.8**
1.0 Hz	363.1 ± 9.1	406.8 ± 8.3*	378.0 ± 7.4	379.4 ± 5.3**	333.0 ± 7.0**
2.0 Hz	318.2 ± 5.3	337.7 ± 5.6'	329.5 ± 4.3	327.6 ± 4.2**	285.3 ± 5.3**

* Significantly different control ($p < 0.05$).
** Significantly different from STZ-diabetic ($p < 0.05$).

when stimulation frequency was increased to either 1.0 or 2.0 Hz. Treating control, non-diabetic animals with Ag had no significant impact on myocyte contractile kinetics at 0.5, 1.0 and 2.0 Hz. Contractile parameters of myocyte from euglycemic animals were similar to that of control animals.

3.4. Relative levels of MHC

Fig. 3 shows steady-state mRNA levels (panel A), electrophoretic mobilities of MHC from control and STZ-diabetic animals (panel B), relative levels of total MHC and MHC-β in hearts from C, D, Ag-C, Ag-D and Ins-D animals (panels C and D). In this study we found that steady-state level of mRNA encoding MHC-α was 50% greater ($p < 0.05$) than that of MHC-β in hearts of control animals and the reverse was found for MHC transcripts following 8 weeks of diabetes (Fig. 3A). Mass spectrometric analysis also revealed that MHC-α is the dominant isozyme in hearts from control animals, accounting for 79% of total MHC protein (Fig. 3B, graph below). The electrophoretogram in Fig. 3B (upper) also shows that MHC-α runs slightly slower than MHC-β on denaturing gradient polyacrylamide gels.

Using the F59 monoclonal antibody, we found that total MHC protein was not altered during diabetes (Fig. 3C). However, the amount of MHC-β isozyme (S58 antibodies) was higher in hearts from STZ-diabetic animals (Fig. 3D), consistent with mRNA and mass spectrometry data. Ag treatment did not alter either total MHC or the composition of MHC isozymes in hearts of both control and STZ-diabetic animals (panels C and D). Insulin therapy (euglycemic) restored MHC-α-as the dominant MHC isozyme in heart.

3.5. Syneresis

Representative time course recordings (panel A) and mean data (±SEM, panel B) of strong myosin–actin interactions (syneresis) after addition of 1 mM ATP to actomyosin gels in a buffer containing ≈5–10 μM free Ca^{2+} are shown in Fig. 4. Following addition of ATP, the rate of absorbance change of actomyosin gels from STZ-diabetic rat hearts was 7.2× slower than that from control animals (0.014 ± 0.002 absorbance units/s *vs* 0.102 ± 0.004 absorbance units/s). Time to peak absorbance was also delayed (Fig. 4A) and peak absorbance was significantly ($p < 0.05$) lower than controls (ΔAbs = 0.06 ± 0.02 *vs* ΔAbs = 0.18 ± 0.03 for control), consistent with a decrease in extent of cell shortening. Ag treatment blunted reductions in rate of change of absorbance and increase change in absorbance (0.056 ± 0.003 absorbance units/sec and ΔAbs = 0.12 ± 0.01, respectively) induced by diabetes. Ag treatment had minimal impact on syneresis in control animals. However, in six out of eight experiments, basal absorbances of actomyosin gels from Ag-C animals were higher than those from C, STZ and Ag-D animals (Fig. 4A (■)), and dissociation of cross-bridges (absorbance decay) were also faster. Mean change in peak absorbance following ATP addition ± SEM are represented in Fig. 4B. Insulin therapy restored syneresis in diabetic animals to near control values.

3.6. Actomyosin ATPase activity

Fig. 5 shows actomyosin Ca^{2+}-ATPase (A) and Mg^{2+}-sensitive ATPase (B) activities in hearts of age-matched control and STZ-induced diabetic rats in the absence and presence of Ag and from euglycemic diabetic animals. The results show that the steady-state Ca^{2+}- and Mg^{2+}-sensitive ATPase activities were lower in actomyosin preparations isolated from STZ-induced diabetic rat hearts compared with actomyosin isolated from hearts of age-matched controls. Ag treatment blunted the decrease in Ca^{2+}-sensitive ATPase activity, but it had no effect on Mg^{2+}-sensitive ATPase activity. In these studies, treating control animals with Ag treatment did not have any significant effect on Ca^{2+}-sensitive ATPase activity, but it increased Mg^{2+}-sensitive ATPase activity. Insulin therapy of diabetic animals restored actomyosin activities to near control values.

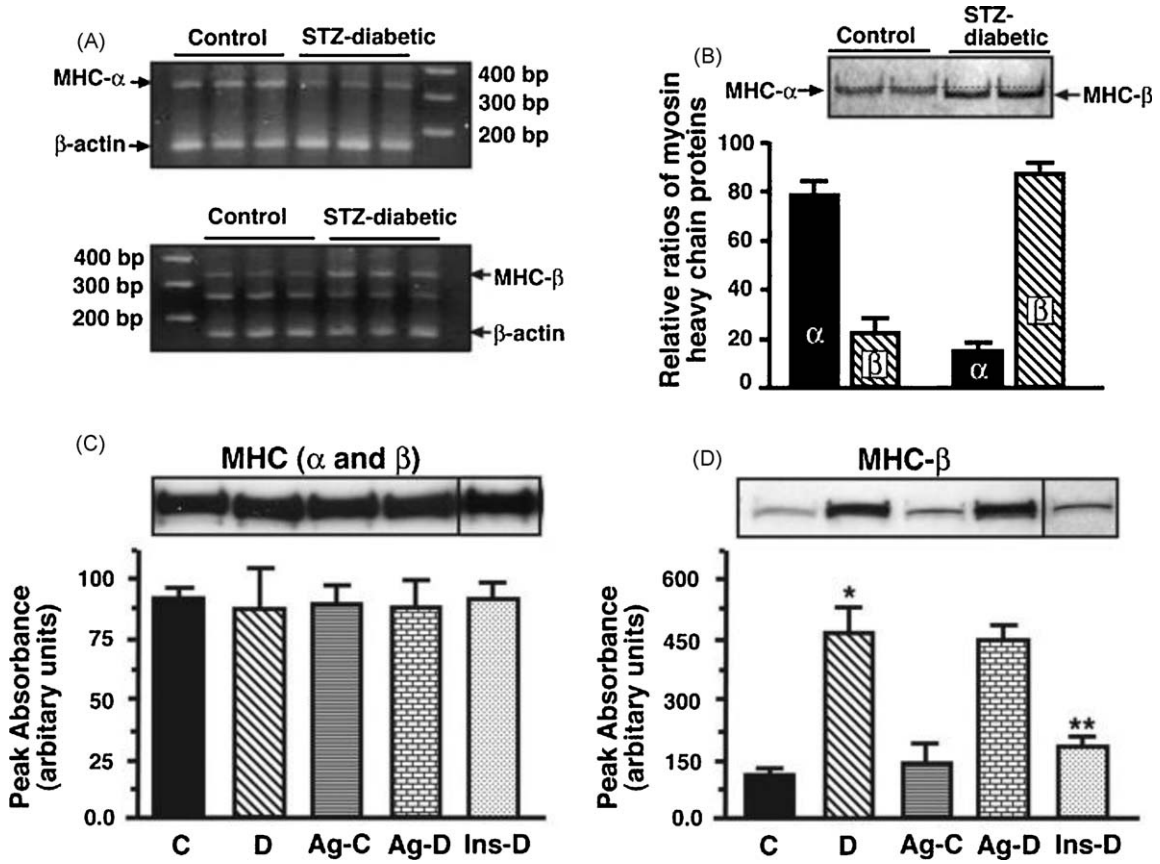

Fig. 3. Panel A shows relative levels of mRNA encoding MHC-α and MHC-(in hearts from control and STZ-diabetic. Panel B (upper) shows electrophoretic mobilities of MHC-α and MHC-(. Panel B (below) also shows relative levels of MHC-α and MHC-(inhearts from control and STZ-diabetic rats. Panel C (upper) shows a representative autoradiogram used to determine relative levels of total MHC in hearts from control (C), STZ-diabetic (D), Ag-treated control (Ag-C), Ag-treated STZ-diabetic (Ag-D) and insulin-treated STZ-diabetic (Ins-D) rats. F59 MHC antibodies were used for these studies. Graph below represent the mean ± SEM. obtained from six separate actomyosin preparations grouper group. Panel D shows a representative autoradiogram used to determine relative levels of MHC-(in hearts from control (C), STZ-diabetic (D), Ag-treated control (Ag-C), Ag-treated STZ-diabetic (Ag-D) and insulin-treated STZ-diabetic (Ins-D) rats. Western blots were performed using S58 MHC antibodies. Graph below represent the mean ± SEM for six different actomyosin preparations from each group. (*) Significantly ($p < 0.05$) different from control.

3.7. Mass spectrometry

3.7.1. Mass spectrometry

Digestion of MHC from control animals with trypsin afforded 212 distinct $M+H^+$ between 700 and 3000 Da using MALDI-TOF mass spectrometry. These $M+H^+$ corresponded to peptides that spanned the entire range of rat MHC (similar for MHC-α and MHC-β). Mass differences were ≤117 parts per million. Peptides with a molecular weight greater than 3000 Da were not assayed as they generally have low ionization efficiencies and/or were not extracted from the gel strip. Of these 212 peptides observed ($M+H^+$), 84 (39%) corresponded to non-miscleaved consensus trypsin peptides from rat MHC-α and 83 (39%) corresponded to non-miscleaved consensus trypsin peptides rat MHC-β. Compar-

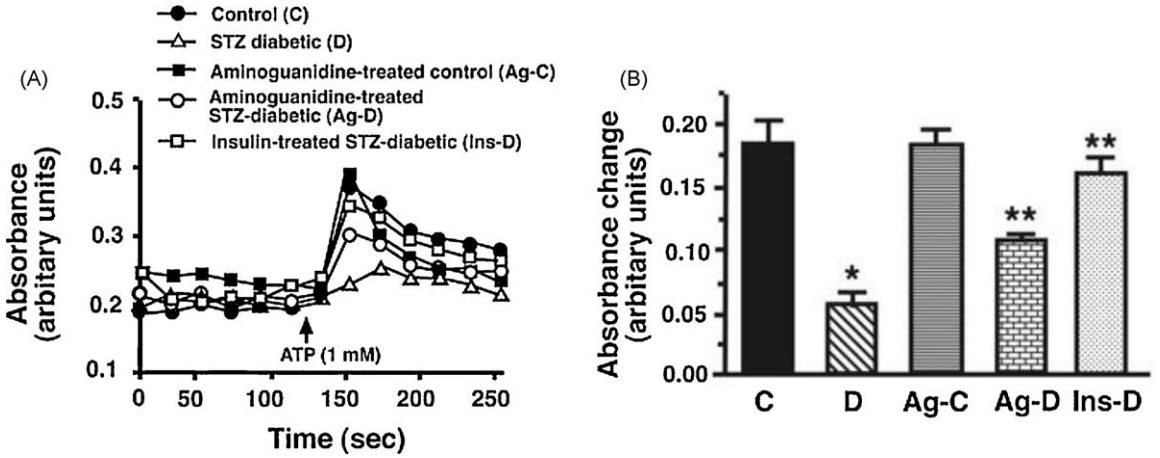

Fig. 4. Panel A shows Ca^{2+}-sensitive ATPase activity and panel B show Mg^{2+}-sensitive ATPase activity for actomyosin isolated from control (C), STZ-diabetic (D), Ag-treated control (Ag-C), Ag-treated STZ-diabetic (Ag-D) and insulin-treated STZ-diabetic (Ins-D) rat hearts. Values shown are mean ± SEM for six different actomyosin preparations for each group. (*) Significantly ($p < 0.05$) different from control. (**) Significantly different ($p < 0.05$) from STZ-diabetic.

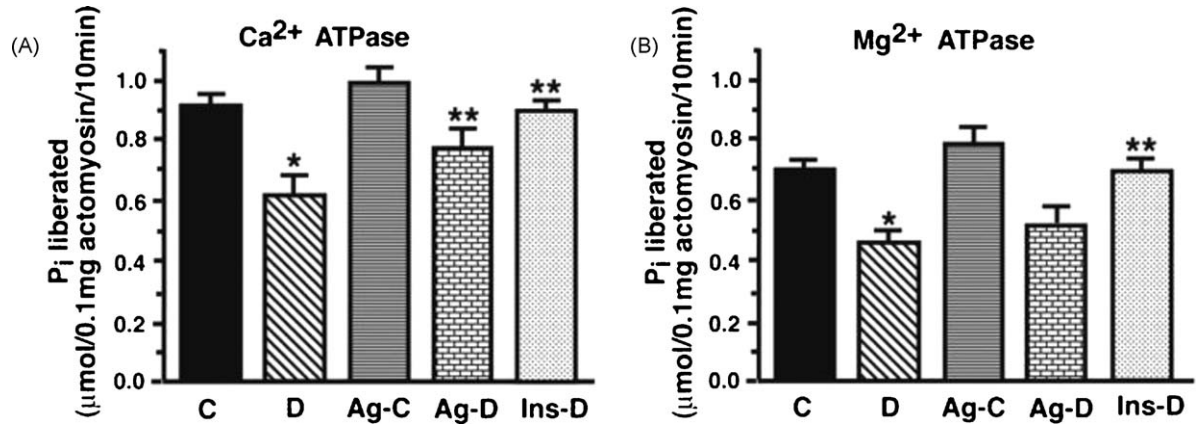

Fig. 5. Panel A shows representative absorbance traces used to assess syneresis of MHC following addition of ATP (1 mM). Panel B show mean ± SEM for eight experiments done using seven different actomyosin preparations per each group. (*) Significantly different from control ($p < 0.05$). (**) Significantly different from STZ-diabetic ($p < 0.05$).

ison of intensities of peptides unique to MHC-α ($M+H^+$ of 832.40, 868.45, 1130.58, 1498.81, 1523.82, 1650.86, 1711.90) and MHC-β $M+H^+$ = 855.45, 985 28357 7 44 76, 1740.92, 1878.95) suggests a relative MHC-α to MHC-β ratio of about 80:20 in control hearts Fig. 3B, consistent with published literature [12,13].

Digestion of MHC from STZ-diabetic rat hearts with trypsin afforded 21% less peptides (167 $M+H^+$) with masses between 700 and 3000 Da (Fig. 6A). Of these, 70 (42%) corresponded to non-miscleaved consensus trypsin peptides from rat MHC-α and 77 (46%) corresponded to non-miscleaved consensus trypsin peptides

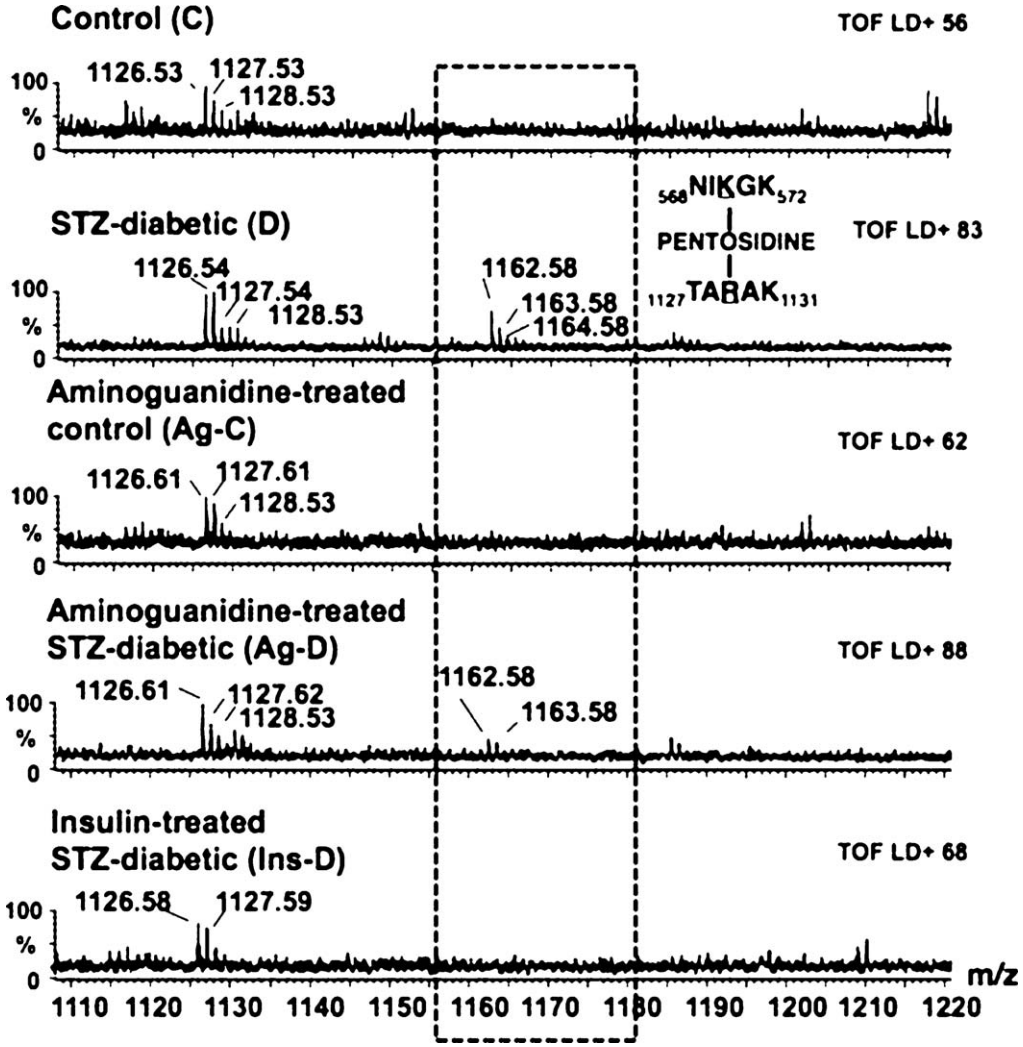

Fig. 6. Shows alignment of a segment of MALDI-TOF mass spectra obtained following trypsin digestion of MHC from control (C), STZ-diabetic (D), Ag-treated control (Ag-C), Ag-treated STZ-diabetic (Ag-D) and insulin-treated STZ-diabetic (Ins-D) rat hearts. The STZ-diabetic sample shows a prominent peak at 1162.58 Da (1163.58 Da and 1163.58 Da are isotopic mass peaks) that is not seen in either control or Ag-treated control sample. Using our in-house PERLscript, this peak was assigned to $_{568}$NI**K**GK$_{572}$ and $_{1127}$TA**R**AK$_{1131}$ crosslinked together by pentosidine.

Table 3
Peptides from MHC with carbonyl adducts. The bolded, underlined letters in the left panel indicate the amino acid modified and the subscripted numbers indicate the location of the peptide. The isozyme and sample type are also listed in parentheses. The type of adduct is listed in the second column. The theoretical, measured and delta mass difference is listed in the other columns.

Amino acid sequence of peptides detected with carbonyl modification	Type of carbonyl modification	Theoretical mass (M^+H^+) of carbonyl modified peptide (Da)	Measured mass (M^+H^+) of carbonyl modified peptide (Da)	Delta mass difference (Da)
$_{1094}$IEDEQALGSQLQ**K**K$_{1107}$ (MHC-β from D)	Carboxymethlysine	1644.86	1644.78	−0.08
$_{1643}$VPADI**R**LTSIK$_{1652}$ (MHC-α from D)	Carboxymethlysine	1217.69	1217.60	−0.09
$_{1269}$SVNDLT**R**QR$_{1277}$ (MHC-β from D, Aq-D)	Imidazolone A	1232.61	1232.65	+0.04
$_{1609}$NEAL**R**VK$_{1615}$ (MHC-α, MHC-β from D)	Imidazolone A	973.51	1162.53	+0.02
$_{398}$GLCHP**R**VKVGNEYVTK$_{413}$ (MHC-α from D, Ag-D, Ins-D)	Imidazolone B	1941.98	1941.99	+0.01
$_{273}$FHGT**K**VFFK$_{281}$ (MHC-β from D, Ag-D)	Pyralline	1211.67	1211.59	−0.08
$_{969}$HATEN**K**VKNLTEEMAGLDEIIVK$_{991}$ (MHC-β from D)	Pyralline	2690.36	2690.52	−0.12
$_{1304}$G**K**LTYTQQLEDLK$_{1316}$ (MHC-β from D)	Pyralline	1644.84	1644.78	−0.06
244FG**K**FIR249 (MHC-α from D, Ag-D)	AFGP	1036.52	1036.52	+0.00
$_{1458}$LELDDVTSHMEQII**K**AK$_{1472}$ {MHC-α from D, Ag-D, Ins-D)	AFGP	2240.09	2240.10	+0.01
$_{795}$GQLMRIEF**K**K$_{804}$ (MHC-α from D, Ag-D)	Amadori product	1411.71	1411.68	−0.03
$_{654}$ENLN**K**LMTNLR$_{664}$ (MHC-α from D)	Amadori product	1507.73	1507.73	0.00
$_{568}$NI**K**GK$_{572}$ | $_{1127}$TA**R**AK$_{1131}$ (MHC-β from D, Ag-D)	Pentosidine	1162.59	1162.57	−0.02
$_{854}$EEFG**R**VK$_{860}$ | $_{1215}$Q**K**LEK$_{1219}$ (MHC-α and MHC-β from D)	Pentosidine	1566.76	1689.75	−0.01

rat MHC-β. Comparison of intensities of peptides unique to MHC-α and MHC-β suggest relative ratio of about 12:88 in STZ-diabetic hearts.

Digestion of MHC from Ag-treated control hearts with trypsin afforded 210 peptides between 700 and 3000 Da. Of these, 94, (46%) corresponded to non-miscleaved consensus trypsin peptides from rat MHC-α and 93 (45%) corresponded to non-miscleaved consensus trypsin peptides rat MHC-β. Comparison of intensities of peptides unique to MHC-α and MHC-β suggest relative ratio of 75:25 in Ag-treated control hearts. The majority of peptides in Ag-treated samples were identical to those found in control samples.

Digestion of MHC isolated from Ag-treated STZ-diabetic rat hearts with trypsin afforded 188 peptides between 700 and 3000 Da (Fig. 6A). Of these, 78 (41%) corresponded to non-miscleaved consensus trypsin peptides from rat MHC-α and 77 (40%) corresponded to non-miscleaved consensus trypsin peptides rat MHC-β. Non-miscleaved peptides found on MHC isolated from STZ-diabetic rat hearts were also consistently found on MHC isolated from aminoguanidine-treated STZ-diabetic rat hearts. Comparison of intensities of peptides unique to MHC-α and MHC-β suggest a relative ratio of ratio of 13:87 in Ag-treated STZ-diabetic samples.

Digestion of MHC from Ins-D with trypsin afforded 213 peptides between 700 and 3000 Da. Of these, 88 (41%) corresponded to non-miscleaved consensus trypsin peptides from rat MHC and 89 (42%) corresponded to non-miscleaved consensus trypsin peptides rat MHC-β. Comparison of intensities of peptides unique to MHC-α and MHC-β suggest relative ratio of 80:20 in Ins-D hearts.

The reduced number of trypsin-derived MHC peptides in STZ-diabetic samples suggests that some lysine and/or arginine residues may be unavailable or resistant to trypsin's action. A PERLscript was then used to search the MALDI-TOF mass data files to determine if any of the $M+H^+$ represent MHC peptides modified with carbonyl adducts, and if so, what type of adduct and where it is located on the protein. As an example, a search of MALDI-TOF mass files revealed a monoisotopic mass of 1162.58 Da was prominent in STZ-diabetic sample (Fig. 6). Since no peptide generated from digestion of MHC with trypsin (even with up to three miscleavages) has a $M+H^+$ of 1162.57 ± 0.5 Da, this peptide was identified as likely candidate with adduct formation. Using our PERLscript, an $M+H^+$ of 1162.57 Da could result from $_{568}$NI**K**GK$_{572}$ and $_{1127}$TA**R**AK$_{1131}$ crosslinked together by pentosidine. Subjecting the 1162.57 Da peak to ionization (fragmentation) showed peaks at 560.35, 546.33 and 274.16, corresponding to the M+1 ion for NIKGK and the M+1 and M+2 ions for TARAK, respectively. Table 3 shows the list of MHC peptides found to contain non-crosslinking and cross-linking carbonyl adducts.

3.8. Confirmation of pentosidine adducts on MHC

Western blots employing pentosidine antibodies were also conducted to confirm the presence of pentosidine adducts found using mass spectrometry on MHC. Fig. 7 shows that for the same protein load, MHC from STZ-diabetic animals contains ≥3 times

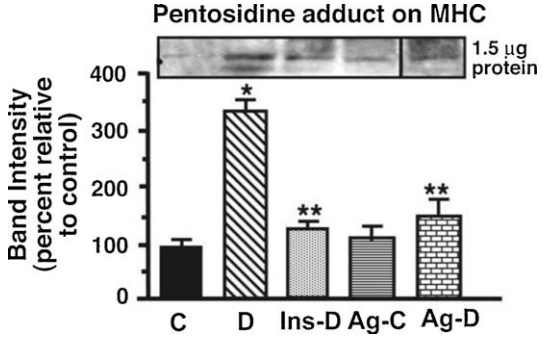

Fig. 7. Relative levels of pentosidine adduct in hearts from control (C), STZ-diabetic (D), Ag-treated control (Ag-C), Ag-treated STZ-diabetic (Ag-D) and insulin-treated STZ-diabetic (Ins-D) rat hearts. The graph below represents the mean ± SEM for five experiments done using five different actomyosin preparations from each group. (*) Significantly different from control ($p < 0.05$). (**) Significantly different from STZ-diabetic ($p < 0.05$).

more immuno-reactive pentosidine adducts than MHC from control animals, consistent with mass spectrometry data. Ag treatment significantly attenuated ($p < 0.05$) formation of pentosidine adducts on MHC. There was a trend toward increased immuno-reactive pentosidine adducts on MHC from Ag-treated control samples. Insulin therapy also reduced the amount of pentosidine adducts on MHC.

4. Discussion

The adult heart produces and consumes a daily ATP mass equivalent to ≥5 times its own mass for maintenance of cellular ionic homeostasis and rhythmic contractions [38]. A significant percentage of this ATP is utilized by MHCs' to form strong cross-bridges with actin for generation of the power stroke. Despite greater than 93% sequence homology, the ATPase activities of MHC-α and MHC-β vary almost three fold due to a divergence in amino acids residues between positions 623 and 640 [39]. While relative ratios of these two isozymes vary in different regions of the heart (atria *vs* ventricle), the tendency is always to shift toward the lower activity MHC-β under chronic stressful conditions, as a way to increase the efficiency and economy of force generation [40]. One of these chronic stressors is type 1 diabetes mellitus. While pharmacologic strategies and lifestyle management have significantly improved the ability of individuals with diabetes to maintain near normal glycemia and increase circulating thyroid hormones, heart failure continues to be a major cause of morbidity and mortality in individuals with diabetes mellitus.

The principal finding of the present study is that in addition to isozyme switching, long-lived MHC isozymes also undergo post-translational modifications by RCS during diabetes and these modifications reduces their activities further. This conclusion is based on strong correlative biochemical, functional, mass spectrometry and integrative data. While the impact of these adducts is likely to be minimal on proteins that turn over quickly, proteins with long-half lives such as MHC are especially vulnerable as adducts will accumulate on them and eventually impairing the rate of its timed conformational changes needs to hydrolyze ATP and generate the power stroke [8,10]. We earlier found carbonyl adducts on two other long-lived, intracellular Ca^{2+} cycling proteins, namely type 2 ryanodine receptor and sarco(endo)plasmic Ca^{2+}-ATPase [35,36].

In agreement with earlier studies [28,30] in this study we also found that diabetes reduces cardiac and myocyte contractile kinetics. We also confirmed the increase in expression of ventricular MHC-β and reductions in actomyosin Ca^{2+}-sensitive ATPase, Mg^{2+}-sensitive ATPase activities and strong binding with actin (syneresis) [11–14,41]. What is unique about the present study is that it shows for the first time the presence of specific non-crosslinking carbonyl adducts (CML, imidazolone A, imidazolone B, pyralline, AGFP and Amadori) on ventricular MHC. It also identifies the locations of these adducts on MHC. Non-crosslinking adducts were found with the head region, in proximity to the junction between the head and the rod region, so called S2 region and within the intertwined tail.

In addition to non-crosslinking adducts, we also found for the first time elevated levels of crosslinking pentosidine adducts on MHC using both mass spectrometry and Western blots employing a pentosidine-specific monoclonal antibody. These adducts were formed by crosslinking amino acid residues within the head domain and upper S2 region located in the rod segment. How peptides from these two distant regions of MHC crosslink with each other during diabetes is not clear at this time. What we do know, however, is that during diabetes, remodeling of the contractile apparatus occurs and as a result some thick filaments undergo depolymerization into inactive myosin monomers [42]. Burgess et al. [42] also suggested that the long tail of these inactive monomers could achieve a folded conformation and this could bring the S2 and head domains closer together. It is also possible that the tail of one depolymerized myosin monomer could come in close contact the head of another.

Having uncovered the presence of carbonyl adducts on MHC, the next step was to show that these adducts are functionally important or an epiphenomenon of diabetes. For this we used Ag since its guanidinium moiety makes it an excellent scavenger of RCS and prevent formation of carbonyl adducts including advanced glycation end products [29,43,44]. Ag is also an inhibitor of SSAO, the enzyme that synthesizes the potent RCS, methylglyoxal [45]. In this study we found that treatment of STZ-diabetic rats with Ag (1 g/L/day, equivalent to 1.6 g/kg/day) for 6 weeks via drinking water, starting 2 weeks after the onset of diabetes, did not alter either the ventricular composition of MHC or serum T3 levels. Consistent with an earlier report [46], Ag treatment significantly reduced circulating levels of thiobarbituric acid reactants (mainly malondialdehyde) and attenuated the increase in SSAO activity induced by diabetes [45]. Ag treatment also blunted actomyosin Ca^{2+}-sensitive ATPase activity loss and ATP-stimulated syneresis. In this study, Ag treatment did not significantly attenuate actomyosin Mg^{2+}-sensitive ATPase activity loss. However, since there was a trend toward an improvement, it is possible that a longer Ag treatment time is needed to see an effect on this parameter.

Ag treatment also reduced significantly the formation of both non-crosslinking and crosslinking carbonyl adducts on the head, S2 and intertwined rod domains of MHC. Since Ag treatment also improved MHC function without altering the MHC composition, these data strongly suggest that the presence of carbonyl adducts is compromising MHC activity during diabetes. Since carbonyl adducts neutralize basic charges and increase bulk, we hypothesize that these adducts are impairing the rate at which MHC is undergoing conformational changes needed to generate the power stroke.

In this study we did not assess ROS levels and as such we cannot exclude the possibility that improvements in MHC activity seen with Ag treatment could be due, at least in part to a reduction in ROS levels. However, it should also be mentioned that although several studies have found that Ag treatment reduces ROS, other found that it does not. As an example, Coppey et al. [47], found that Ag was ineffective in reducing superoxide production *in vivo*, helping to discerns the effects of RCS from that of ROS, which is also elevated during diabetes. Similarly, some studies suggest that Ag can protect against NO-mediated vasodilation while other studies found no effect [48,49]. It is not clear at this time whether these discrepancies are species or tissue-dependent.

At the level of the myocyte, Ag treatment also blunted decreases in rate of contraction and extent of myocyte shortening, parameters that depend in part on the activity of MHC. Ag treatment also blunted reductions in myocardial fractional shortening, basal and isoproterenol-stimulated rates of left ventricular pressure development and peak left ventricular pressures, similar to that recently shown by Wu et al. [50]. Improvements in contraction kinetics are unlikely to be solely as a result of a reduction in MHC carbonylation. Instead, they are likely to result from decarbonylation (or prevention of carbonylation) of several long-lived proteins involved in myocyte/myocardial contractility, including type 2 ryanodine receptor, titin, etc. It should also be pointed out that Ag treatment did not improve basal and isoproterenol-stimulated cardiac relaxation rates ($-dP/dt$), suggesting that Ag actions were not targeted at sarco(endo)plasmic reticulum Ca^{2+}-ATPase, $Na^{+}Ca^{2+}$ exchanger, collagen and fibronectin, proteins intimately involved in cardiac and myocyte relaxation. The reason for this selectivity of Ag is not clear at this time. Probably other more factors are affecting their function or the potency of Ag to reduce/prevent carbonyl adducts is not sufficient.

In the present study we also found that treating control, non-diabetic animals with Ag significantly lower their heart rates and increase left ventricular end-diastolic pressures. There were also trends toward increases in $\pm dP/dt$. The reason for these cardiac changes are not fully understood at this time, but could be the result of Ag itself reacting with hyperreactive basic residues of some contractile proteins to increase their activity, in a manner similar to which low level of oxidants increase the activity of type 2 ryanodine receptor [51]. Ag-treated control animals also had significantly higher concentrations of serum levels of thiobarbituric acid reactive substances (TBARS) and increased serum activity of serum semicarbazide amine oxidase (SSAO). One of the most prominent thiobarbituric acid reactants measured in serum is malondialdehyde and an increase in its circulating level would indicate that Ag treatment is increasing fatty acid oxidation [52]. The increase in serum SSAO suggests that more membrane-bound SSAO is entering into the circulation. One explanation is that SSAO expression is being upregulated in vascular endothelial cells and more of it is secreted in the circulation [20]. The reason for this is not clear but could be as a result of an increase in blood pressure in Ag-treated rats. These findings may also provide another reason for the lack of interest in clinically developing Ag to scavenger RCS [53].

In conclusion, the present study identifies, for the first time, specific sites on MHC that undergo carbonylation (crosslinking and non-crosslinking) during diabetes. It also showed that treating STZ-diabetic animals with Ag reduced formation of carbonyl adducts and attenuated MHC activity loss. These new data should provide additional insights into mechanism that contributes to the cardiac inotropic loss during diabetes mellitus. They would also suggest that lowering RCS levels could be an important adjunct strategy for reducing cardiac dysfunction during diabetes.

Acknowledgements

This work was supported in part by grants from the Edna Ittner Research Foundation (K.R.B), American Diabetes Association (K.R.B), National Institutes of Health NS-39751 (K.P.P), HL-066446 (G.J.R), HL 090657 and AA 01128 (W.G.M) and HL085061 (K.R.B) and Grant-in-Aid from the Ministry of Education, Science, Sports and Cultures of Japan (Scientific Research grant # 18790619, R.N).

References

[1] Wild S, Roglic G, Green A, Sicree R, King H. Global prevalence of diabetes: estimates for the year 2000 and projections for 2030. Diabetes Care 2004;27(5):1047–53.
[2] Anon. The global challenge of diabetes. Lancet 2008;371(9626):1723.
[3] American Diabetes Association: all about diabetes. Available at http://www.diabetes.org/about-diabetes.jsp [accessed February 2010].
[4] Fang ZY, Prins JB, Marwick TH. Diabetic cardiomyopathy: evidence, mechanisms, and therapeutic implications. Endocr Rev 2004;25(4):543–67.
[5] Janka HU. Increased cardiovascular morbidity and mortality in diabetes mellitus: identification of the high-risk patient. Diabetes Res Clin Pract 1996;30(Suppl.):85–8.
[6] Barral JM, Epstein HF. Protein machines and self-assembly in muscle organization. Bioessays 1999;21(10):813–23.
[7] Rayment I, Rypniewski WR, Schmidt-Bäse K, Smith R, Tomchick DR, Benning MM, et al. Three-dimensional structure of myosin subfragment-1: a molecular motor. Science 1993;261(5117):50–8.
[8] Houdusse A, Szent-Györgyi AG, Cohen C. Three conformational states of scallop myosin S1. Proc Natl Acad Sci USA 2000;97(21):11238–43.
[9] Parmacek MS, Solaro RJ. Biology of the troponin complex in cardiac myocytes. Prog Cardiovasc Dis 2004;47(3):159–76.
[10] Rayment I, Holden HM, Whittaker M, Yohn CB, Lorenz M, Holmes KC, et al. Structure of the actin-myosin complex and its implications for muscle contraction. Science 1993;261(5117):58–65.
[11] Dillmann WH. Diabetes mellitus induces changes in cardiac myosin of rat. Diabetes 1980;29(7):579–82.
[12] Malhotra A, Penpargkul S, Fein FS, Sonnenblick EH, Scheuer J. The effect of streptozotocin-induced diabetes in rats on cardiac contractile proteins. Circ Res 1981;49(6):1243–50.
[13] Dillmann WH. Influence of thyroid hormone administration on myosin ATPase activity and myosin isoenzyme distribution in the heart of diabetic rats. Metabolism 1982;31(3):199–204.
[14] Gupta MP. Factors controlling cardiac myosin-isoform shift during hypertrophy and heart failure. J Mol Cell Cardiol 2007;43(4):388–403.
[15] Bugger H, Abel ED. Rodent models of diabetic cardiomyopathy. Dis Model Mech 2009;2(9–10):454–66.
[16] Chatham JC, Forder C, McNeill JH, editors. The heart in diabetes (developments in cardiovascular medicine). Ist ed., New York: Springer; 1996.
[17] Action to Control Cardiovascular Risk in Diabetes Study Group, Gerstein HC, Miller ME, Byington RP, Goff Jr DC, Bigger JT, Buse JB, et al. Effects of intensive glucose lowering in type 2 diabetes. N Engl J Med 2008;358(24):2545–59.
[18] Anon. Effect of intensive blood-glucose control with metformin on complications in overweight patients with type 2 diabetes (UKPDS 34). UK Prospective Diabetes Study (UKPDS) Group. Lancet 1998;352(9131):854–65.
[19] Baynes JW, Thorpe SR. Role of oxidative stress in diabetic complications: a new perspective on an old paradigm. Diabetes 1999;48(1):1–9.
[20] Obata T. Diabetes and semicarbazide-sensitive amine oxidase (SSAO) activity: a review. Life Sci 2006;79(5):417–22.
[21] Uchida K. Role of reactive aldehyde in cardiovascular diseases. Free Radic Biol Med 2000;28(12):1685–96.
[22] Martin AF, Rabinowitz M, Blough R, Prior G, Zak R. Measurements of half-life of rat cardiac myosin heavy chain with leucyl-tRNA used as precursor pool. J Biol Chem 1977;252(10):3422–9.
[23] Yudkin JS, Cooper MB, Gould BJ, Oughton J. Glycosylation and cross-linkage of cardiac myosin in diabetic subjects: a post-mortem study. Diabet Med 1988;5(4):338–42.
[24] Syrový I, Hodný Z. Non-enzymatic glycosylation of myosin: effects of diabetes and ageing. Gen Physiol Biophys 1992;11(3):301–7.
[25] Snow LM, Lynner CB, Nielsen EM, Neu HS, Thompson LV. Advanced glycation end product in diabetic rat skeletal muscle in vivo. Pathobiology 2006;73(5):244–51.
[26] Ramamurthy B, Höök P, Jones AD, Larsson L. Changes in myosin structure and function in response to glycation. FASEB J 2001;15(13):2415–22.
[27] National Research Council. Guide for the care and use of laboratory animals. Washington, DC: National Academy Press; 1996.
[28] Shao CH, Wehrens XH, Wyatt TA, Parbhu S, Rozanski GJ, Patel KP, et al. Exercise training during diabetes attenuates cardiac ryanodine receptor dysregulation. J Appl Physiol 2009;106(4):1280–92.
[29] Li YM, Steffes M, Donnelly T, Liu C, Fuh H, Basgen J, et al. Prevention of cardiovascular and renal pathology of aging by the advanced glycation inhibitor aminoguanidine. Proc Natl Acad Sci USA 1996;93(9):3902–7.
[30] Shao CH, Rozanski GJ, Patel KP, Bidasee KR. Dyssynchronous (non-uniform) Ca^{2+} release in myocytes from streptozotocin-induced diabetic rats. J Mol Cell Cardiol 2007;42(1):234–46.
[31] Danzi S, Ojamaa K, Klein I. Triiodothyronine-mediated myosin heavy chain gene transcription in the heart. Am J Physiol Heart Circ Physiol 2003;284(6):H2255–62.
[32] Ash AS, Besch Jr HR, Harigaya S, Zaimis E. Changes in the activity of sarcoplasmic reticulum fragments and actomyosin isolated from skeletal muscle of thyroxine-treated cats. J Physiol 1972;224(1):1–19.
[33] Bhan AK, Scheuer J. Effects of physical training on cardiac myosin ATPase activity. Am J Physiol 1975;228(4):1178–82.
[34] Lanzetta PA, Alvarez L, Reinach PS, Candia OA. An improved assay for nanomole amounts of inorganic phosphate. Anal Biochem 1979;100:95–7.
[35] Bidasee KR, Nallani K, Yu Y, Cocklin RR, Zhang Y, Wang M, et al. Chronic diabetes increases advanced-glycation end products on cardiac ryanodine receptors (RyR2). Diabetes 2003;52(7):1825–36.
[36] Bidasee KR, Zhang Y, Shao CH, Wang M, Patel KP, Dincer UD, et al. Diabetes increases formation of advanced glycation end products on sarco(endo)plasmic reticulum Ca2+-ATPase. Diabetes 2004;53(2):463–73.
[37] Miyazaki K, Nagai R, Horiuchi S. Creatine plays a direct role as a protein modifier in the formation of a novel advanced glycation end product. J Biochem 2002;132(4):543–50.
[38] Sack MN. Type 2 diabetes, mitochondrial biology and the heart. J Mol Cell Cardiol 2009;46(6):842–9.
[39] Weiss A, Leinwand LA. The mammalian myosin heavy chain gene family. Annu Rev Cell Dev Biol 1996;12:417–39.
[40] Schaub MC, Hefti MA, Zuellig RA, Morano I. Modulation of contractility in human cardiac hypertrophy by myosin essential light chain isoforms. Cardiovasc Res 1998;37(2):381–404.
[41] Garber DW, Neely JR. Decreased myocardial function and myosin ATPase in hearts from diabetic rats. Am J Physiol 1983;244(4):H586–91.
[42] Burgess SA, Yu S, Walker ML, Hawkins RJ, Chalovich JM, Knight PJ. Structures of smooth muscle myosin and heavy meromyosin in the folded, shutdown state. J Mol Biol 2007;372(5):1165–78.
[43] Chen HJ, Cerami A. Mechanism of inhibition of advanced glycosylation by aminoguanidine in vitro. J Carbohyd Res 1993;12:731–42.
[44] Thornalley PJ. Use of aminoguanidine (Pimagedine) to prevent the formation of advanced glycation endproducts. Arch Biochem Biophys 2003;419(1):31–40.
[45] Yu PH, Zuo DM. Aminoguanidine inhibits semicarbazide-sensitive amine oxidase activity: implications for advanced glycation and diabetic complications. Diabetologia 1997;40(11):1243–50.
[46] Yildiz O, Ozata M, Ozkardeş A, Deniz G, Yildirimkaya M, Corakçi A, et al. Comparison of the effects of aminoguanidine and L-carnitine treatments on somatosensorial evoked potentials in alloxan-diabetic rats. Naunyn Schmiedebergs Arch Pharmacol 1996;354(4):526–31.

[47] Coppey LJ, Gellett JS, Davidson EP, Dunlap JA, Yorek MA. Effect of treating streptozotocin-induced diabetic rats with sorbinil, myo-inositol or aminoguanidine on endoneurial blood flow, motor nerve conduction velocity and vascular function of epineurial arterioles of the sciatic nerve. Int J Exp Diabetes Res 2003;3(1):21–36.
[48] Ozyazgan S, Unlucerci Y, Bekpinar S, Akkan AG. Impaired relaxation in aorta from streptozotocin-diabetic rats: effect of aminoguanidine (AMNG) treatment. Int J Exp Diabetes Res 2000;1(2):145–53.
[49] Brooks BA, Heffernan S, Thomson S, McLennan SV, Twigg SM, Yue DK. The effects of diabetes and aminoguanidine treatment on endothelial function in a primate model of type 1 diabetes. Am J Primatol 2008;70(8):796–802.
[50] Wu MS, Liang JT, Lin YD, Wu ET, Tseng YZ, Chang KC. Aminoguanidine prevents the impairment of cardiac pumping mechanics in rats with streptozotocin and nicotinamide-induced type 2 diabetes. Br J Pharmacol 2008;154(4):758–64.
[51] Xu L, Eu JP, Meissner G, Stamler JS. Activation of the cardiac calcium release channel (ryanodine receptor) by poly-S-nitrosylation. Science 1998; 279(5348):234–7.
[52] Vajdovich P, Gaál T, Szilágyi A. Changes of lipid peroxidation parameters in dogs with alloxan diabetes. Acta Physiol Hung 1993;81(4):317–26.
[53] Khalifah RG, Chen Y, Wassenberg JJ. Post-Amadori AGE inhibition as a therapeutic target for diabetic complications: a rational approach to second-generation Amadorin design. Ann NY Acad Sci 2005;1043:793–806.